ROYAL SOCIETY OF CHEMISTRY

COMMUNICATION

CrossMark
click for updates

A supermolecular building layer approach for gas separation and storage applications: the eea and rtl MOF platforms for CO₂ capture and hydrocarbon separation†

Zhijie Chen, Karim Adil, Łukasz J. Weseliński, Youssef Belmabkhout and Mohamed Eddaoudi*

The supermolecular building layer (SBL) approach was employed to deliberately synthesize five novel metal–organic frameworks (**1–5**) with an exposed array of amide or amine functionalities within their pore system. The ability to decorate the pores with nitrogen donor moieties offers potential to evaluate/elucidate the structure–adsorption property relationship. Two MOF platforms, **eea**-MOF and **rtl**-MOF, based on pillaring of **kgm**-a or **sql**-a layers with heterofunctional 3-connected organic building blocks were targeted and constructed to purposely introduce and expose the desired amide or amine functionalities. Interestingly, gas adsorption properties of **eea**-MOF-4 (**1**) and **eea**-MOF-5 (**2**) showed that by simply altering the nitrogen donor position within the ligand, it is possible to relatively reduce the pore size of the related **eea**-MOF material and subsequently increase the associated CO_2 uptake. The slightly confined pore space in **2**, relative to **1**, has enabled an enhancement of the pore local charge density and thus the observed relative increase in the CO_2 and H_2 isosteric heat of adsorption (Q_{st}). In addition, light hydrocarbon adsorption studies revealed that **2** is more selective toward C_2H_6 and C_3H_8 over CH_4 than **1**, as exemplified for $C_2H_6 : CH_4$ (5 : 95) or $C_3H_8 : CH_4$ (5 : 95) binary gas mixtures.

1. Introduction

In recent years, metal–organic frameworks (MOFs) have emerged as an attractive class of solid-state materials owing to their associated exceptional wide range of properties pertinent

Functional Materials Design, Discovery and Development Research Group (FMD³), Advanced Membranes and Porous Materials Center (AMPM), Division of Physical Sciences and Engineering, King Abdullah University of Science and Technology (KAUST), Thuwal 23955-6900, Kingdom of Saudi Arabia. E-mail: mohamed.eddaoudi@kaust.edu.sa

to gas storage/separation,[1–7] catalysis,[8] surface chemistry and sensors[9,10] and drug controlled release.[11–13] Importantly, advances in MOF crystal chemistry offer potential to ideally practice the building block approach based-assembly for the construction of a given MOF with desired and appropriate chemical and structural features for specific applications.[14] Namely, the ability to design and construct a MOF with the appropriate pore size, shape and functionality offers prospects to rationally correlate properties with the structure, and subsequently access appropriate MOF platforms[15] that can address some difficult and energy intensive gas separations, *e.g.* CO_2 capture[16,17] and hydrocarbon separation.[18,19] Nevertheless, the unequivocal prediction of a given MOF structure prior to its assembly remains an ongoing challenge; our group has recently published an elaborate tutorial review highlighting distinct strategies that can assist/aid chemists to rationally assemble desired functional MOFs.[20]

A unique and powerful assembly strategy, detailed in the aforementioned review, is based on the use of pre-targeted 2-periodic MOF layers as supermolecular building layers (SBLs) for the deliberate construction of 3-periodic functional MOFs.[20] In the present study, we employed the SBL approach to deliberately synthesize functional MOFs with an exposed array of amide or amine functionalities within their pore system. Specifically, two MOF platforms based on (3,6)-connected nets with **eea** and **rtl** underlying topologies were targeted, *i.e.* **eea**-MOF and **rtl**-MOF platforms.[21–24] The elected two MOF platforms consist of inter-connected layers and thus can be regarded as 3-periodic MOFs based on pillared 2-periodic SBLs.[20] Indeed, our research group has employed successfully the SBL approach to target and construct isoreticular **tbo**-MOFs,[25] exhibiting large surface areas and exceptional CH_4 storage working capacity for stationary applications.[18] Similarly, other 3-periodic porous MOFs can be potentially targeted *via* pillaring SBLs based on one of the sole five edge-transitive 2-periodic nets: **sql** (square lattice), **kgm** (Kagomé), **hcb** (honeycomb), **kgd** (Kagomé dual) and **hex** (hexagonal lattice).[15] Noticeably, augmenting the aforementioned nets, *i.e.* replacing a vertex with a

6276 | *J. Mater. Chem. A*, 2015, 3, 6276–6281

This journal is © The Royal Society of Chemistry 2015

vertex figure, reveals only two distinct possibilities for the assembly of squares into edge-transitive 2-periodic nets, namely **sql**-a and **kgm**-a.

The distinctive **kgm**-a and **sql**-a nets can be regarded as ideal blueprints to target 2-periodic MOFs based on the assembly of square building units, derived from well-known metal paddle-wheel clusters as molecular building blocks (MBBs).[26] Subsequently, the resultant MOF layers can be perceived as SBLs that are amenable to pillaring through 2-, 3-, 4- or 6-connected organic building blocks for the construction of desired 3-periodic MOF platforms.[20]

Here, the ligand-to-axial (L-A) pillaring strategy, successfully introduced by us[21] and demonstrated by others,[23,24] has been employed to introduce the desired functionality into the resultant MOF *via* pillar moieties. Purposely, triangular hetero-functional ligands were conceived to contain concurrently (i) the isophthalic moiety, needed for the formation of the layers in combination with dinuclear cluster paddlewheel MBBs, (ii) nitrogen donor moiety necessary for connecting neighboring layers *via* its coordination to an apical position in the dinuclear cluster, and (iii) specific functional groups such as acetylamide[27–30] or amines[31,32] that offer potential to enhance the affinity between CO_2 molecules and the pore system in the resultant (3,6)-connected 3-periodic MOF.

Indeed, 3-connected organic building blocks (5-R-isophthalic acid with R = isonicotinamido, nicotinamido, pyridin-4-ylamino, pyridin-3-ylamino, and pyrimidin-5-ylamino) were synthesized and employed in combination with the dinuclear copper paddlewheel to yield the targeted **eea**-MOF-4 (**1**), **eea**-MOF-5 (**2**), **rtl**-MOF-2 (**3**), **rtl**-MOF-3 (**4**) and **rtl**-MOF-4 (**5**). Interestingly, gas adsorption properties of **eea**-MOF-4 (**1**) and **eea**-MOF-5 (**2**) showed that by simply altering the nitrogen donor position within the ligand, it is possible to relatively reduce the pore size of the related **eea**-MOF material and subsequently increase the associated CO_2 uptake and relative affinity toward light hydrocarbons.

2. Results and discussion

The solvothermal reaction of copper nitrate and 5-(iso-nicotinamido)isophthalic acid (H_2L1) in *N,N'*-dimethylacetamide (DMA)/acetic acid (HOAc) at 115 °C for 24 h yielded green block microcrystals. The structure of the as-synthesized compound was determined by single-crystal X-ray diffraction (SCXRD) and formulated as $Cu(L1) \cdot (solv)_x$ (**1**), **eea**-MOF-4 (Fig. 1). The phase purity of the crystalline material was confirmed by similarities between the experimental and calculated powder X-ray diffraction (PXRD) patterns (ESI, Fig. S9†).

The resultant 3-periodic **eea**-MOF-4 can be regarded as **kgm**-MOF layers interconnected *via* an L-A pillaring approach, where L1 serves as a 3-connected node and the paddlewheel MBB as a 6-connected octahedral building unit. Topological analysis reveals that **1** has the anticipated **eea** underlying net topology (ESI, Fig. S7†). It is worth noting that while writing the present manuscript, a similar compound appeared in the literature.[30]

The **kgm**-MOF sheets in **1** are pillared in an arrangement where pairs of three-membered ring windows of neighboring
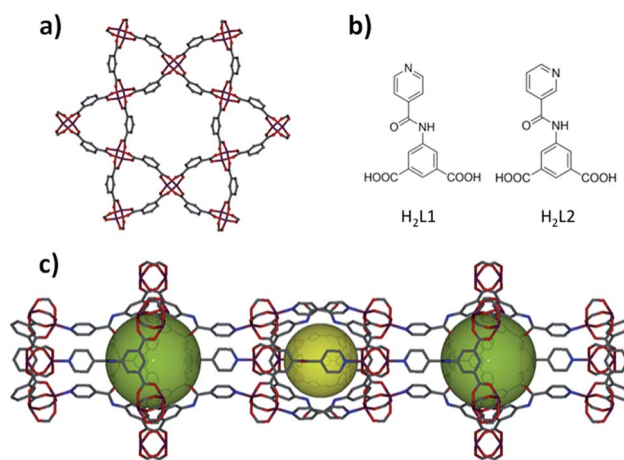

Fig. 1 (a) Layer segment of a **kgm**-MOF. (b) Left: 5-(isonicotinamido) isophthalic acid (H_2L1) and right: 5-(nicotinamido)isophthalic acid (H_2L2). (c) Hourglass-shaped channels with two primary types of cavities. C = gray, O = red, N = blue, Cu = plum; H atoms are omitted for clarity.

sheets are further interconnected *via* interfacing six-membered ring windows (*i.e.*, 3, 3, 6, 3, 3) to yield hourglass-shaped channels (Fig. 1c). These hourglass-shaped channels are comprised of two alternating kinds of cavities (7.8 Å and 10.5 Å diameters), one is delimited by neighboring three membered rings and the second is generated from enclosing hexagonal windows by two three-membered ring windows from the two neighboring layers, as shown in Fig. 1. The calculated total accessible volume for the as-synthesized **1**, upon removal of guest solvent molecules, was estimated to be 6887 $Å^3$ per unit cell volume (11 558 $Å^3$) or 59.6% v/v.

The **eea**-MOF platform offers potential to control and fine-tune the pore size *via* shifting the N-donor group of the pyridine rings within the 3-connected organic building block. Accordingly, we synthesized and used 5-(nicotinamido)isophthalic acid (H_2L2) under similar reaction conditions to construct the anticipated isoreticular **eea**-MOF-5 (**2**). The single-crystal analysis confirms the expected crystal structure formulated as $Cu(L2) \cdot (solv)_x$ (Fig. 1). The replacement of isonicotinamide by the nicotinamide group resulted in slight changes in the size and shape of the two cavities (7.6 Å and 9.8 Å diameters).

The experimental PXRD of the bulk material matches perfectly the calculated PXRD pattern based on the crystal structure of **2**, confirming the phase purity of the resultant as-synthesized **2** (ESI, Fig. S9†). The thermogravimetric analysis (TGA) of compounds **1** and **2** reveals the stability of compounds **1** and **2** up to 523 K (ESI, Fig. S11†).

In order to confirm the versatility of the SBL approach for the synthesis of isoreticular MOFs, we synthesized three additional 3-connected organic building blocks (5-R-isophthalic acid with R = pyridin-4-ylamino, pyridin-3-ylamino, and pyrimidin-5-ylamino). The reaction between copper nitrate and 5-(pyridin-4-ylamino)isophthalic acid (H_2L3) in a mixture of *N,N'*-dimethylformamide (DMF), ethanol and water resulted in a 3-periodic MOF, $Cu(L3) \cdot (solv)_x$, **3**, based on a triangular organic building block interconnecting 2-periodic **sql**-MOF layers in a ligand-to-

axial (L-A) pillaring fashion (Fig. 2). Topological analysis reveals that **3** is consistent with the anticipated **rtl** topology, where L3 serves as a 3-connected node and the paddlewheel MBB as a 6-connected node (ESI, Fig. S8†).

The **sql**-a MOF layer comprises square windows where a pair of adjacent benzene moieties in any given four-membered ring points up while the other adjacent pair points down, *i.e.* benzene moieties in the four-membered ring are arranged in a 1,2-alternate fashion. The quadrangular windows of neighboring 2D **sql** MOF layers are superimposed to generate channels (2.9 × 7.1 Å) running along the *c*-axis. The calculated total accessible volume for the as-synthesized **3**, upon removal of guest solvent molecules, was estimated to be 3216 Å³ per unit cell volume (6203 Å³) or 51.9% v/v.

As expected, the reaction between copper nitrate and 5-(pyridin-3-ylamino)isophthalic acid (H_2L4), or 5-(pyrimidin-5-ylamino)isophthalic acid (H_2L5) yielded the formation of two isoreticular **rtl**-MOF materials as a result of L-A pillaring of **sql**-a MOF layers, $Cu(L4)\cdot(solv)_x$ and $Cu(L5)\cdot(solv)_x$, respectively (Fig. 2). Similar to **eea**-MOF-4 and **eea**-MOF-5, the use of different isomers/analogs resulted in slight changes in the associated channel size dimensions (3.55 × 5.6 Å).

The experimental PXRD of the as-synthesized bulk materials matches perfectly the respective calculated PXRD pattern based on the associated crystal structure, confirming the phase purity of the resultant as-synthesized **3–5** (ESI, Fig. S10†).

The permanent porosity of **1** and **2** has been confirmed by argon (Ar) adsorption isotherms at 87 K (Fig. 3). Ar adsorption experiments on compound **1** show a fully reversible type-I isotherm, characteristic of a microporous material with permanent microporosity. The apparent Langmuir surface area of **1** was estimated to be 1860 m² g⁻¹ and the experimental total pore volume derived from the Ar isotherm was found to be
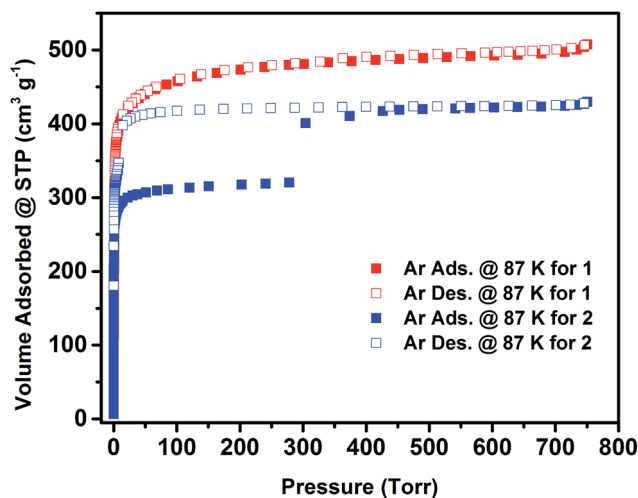

Fig. 3 Low pressure argon adsorption (solid squares) and desorption (open squares) isotherms at 87 K for the acetone exchanged **1** and **2**.

0.65 cm³ g⁻¹, which is in good agreement with the calculated pore volume from the crystal structure (0.66 cm³ g⁻¹). In contrast, **2** displayed an unusual two-step adsorption isotherm with stepwise adsorption behaviour and a noticeable wide-open hysteresis, which can be symptomatic of plausible framework flexibility. The amount of argon adsorbed up to the first plateau was estimated to be ∼320 cm³ g⁻¹, and the total amount of argon adsorbed in the framework was estimated to be ∼430 cm³ g⁻¹, equivalent to an uptake increase of nearly ∼110 cm³ g⁻¹ between the two adsorption plateaus. Accordingly, the apparent Langmuir surface area of compound **2**, determined using the adsorption data leading to the first plateau, was estimated to be 1200 m² g⁻¹. The estimated total pore volume of **2** derived from the Ar isotherm was estimated to be 0.54 cm³ g⁻¹, matching the total uptake at the second plateau, and correlates remarkably with the calculated total pore volume from the crystal structure (0.52 cm³ g⁻¹). Notably, the total pore volume of **2** (0.54 cm³ g⁻¹) is smaller than the total volume of **1** (0.66 cm³ g⁻¹), confirming the contraction of the pore system in **2** as a result of nitrogen position in the pillaring ligand.

The shapes of the Ar adsorption/desorption isotherms at cryogenic temperature suggest a plausible gate effect occurring around 14 mmol g⁻¹ of adsorbed Ar at 87 K. In order to verify the occurrence of this adsorption gate effect, we explored the adsorption of different other probe molecules, namely CO_2, C_3H_8 and $n\text{-}C_4H_{10}$. Markedly, the aforementioned adsorption gate effect was also observed with these probe molecules at relatively low and high pressures (ESI, Fig. S14–S18†).

Interestingly, the adsorbed amounts corresponding to the first plateau were reduced from CO_2 (7 mmol g⁻¹), C_3H_8 (4.2 mmol g⁻¹) to $n\text{-}C_4H_{10}$ (3.75 mmol g⁻¹) in accordance with the increase in the sorbate kinetic diameter and polarizability (ESI, Fig. S19†).

In order to further explore the MOF associated adsorption properties, CO_2, H_2, N_2, and light hydrocarbon adsorption experiments were carried out at various temperatures and pressures. The CO_2 adsorption uptake (298 K) of **1** at 0.15 and 1
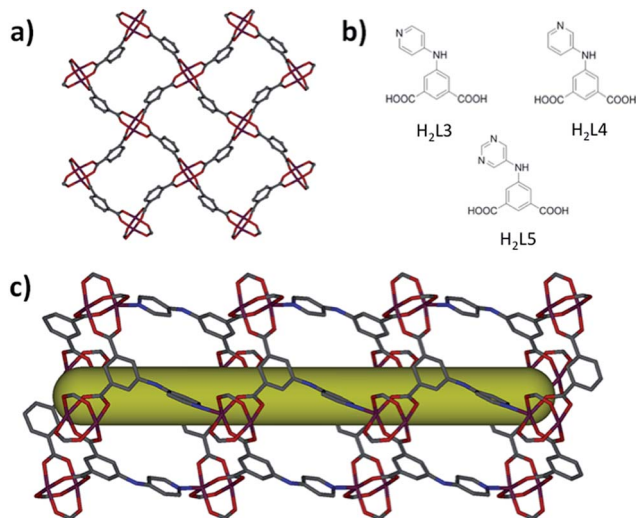

Fig. 2 (a) Layer segment of a **sql**-MOF. (b) Left, up: 5-(pyridin-4-yla-mino)isophthalic acid (H_2L3). Right, up: 5-(pyridin-3-ylamino)iso-phthalic acid (H_2L4). Bottom: 5-(pyrimidin-5-ylamino)isophthalic acid (H_2L5). (c) Projection along the *a*-axis of the **rtl**-MOF-2 displaying channel. C = gray, O = red, N = blue, and Cu = plum; H atoms are omitted for clarity.

6278 | *J. Mater. Chem. A*, 2015, **3**, 6276–6281

This journal is © The Royal Society of Chemistry 2015

bar was 0.56 mmol g^{-1} and 3 mmol g^{-1}, respectively (Fig. 4). By contracting the pore size, the CO_2 adsorption uptake (298 K) of **2** at 0.15 and 1 bar increased by 67% (0.94 mmol g^{-1}) and 50% (4.5 mmol g^{-1}), respectively. The CO_2 adsorption uptake of **2** at 1 bar and 298 K is higher than most of the acylamide functional MOFs.[29] In contrast to the increased uptake of CO_2, **2** shows similar uptake of methane and nitrogen at 298 K to **1**, which can only adsorb limited amounts of CH_4 (0.9 mmol g^{-1}) and N_2 (0.18 mmol g^{-1}) at 298 K and 1 bar. Ideal adsorbed solution theory (IAST)[33] was used to predict the separation factor of equimolar CO_2/CH_4 and CO_2/N_2 (10 : 90) mixtures using experimentally obtained single gas adsorption isotherms (Fig. 5).

IAST selectivity prediction is a valid methodology when the same elaborate model fits matchlessly the experimental data from single gas adsorption isotherms.[34] Accordingly, IAST can be confidently used to evaluate gas selectivities in **eea**-MOFs. Compared with **1**, the predicted separation factors of CO_2/N_2 and CO_2/CH_4 for **2** are significantly improved from 19.2 to 39.3 and from 4.3 to 7.3, respectively. To better understand the energetics of the interaction between CO_2 and associated MOFs, the isosteric heat of adsorption (Q_{st}) over the entire studied range was calculated for **1** and **2** using CO_2 isotherms at 258, 273, 288 and 298 K (ESI, Fig. S14 and S15†). The Q_{st} of CO_2 adsorption for **2** is slightly higher than **1** over the whole range, with the highest point at *ca.* 27.5 over *ca.* 24.6 kJ mol^{-1} (Fig. 4, inset). The Q_{st} of CO_2 adsorption for **2** is relatively high among MOFs without open metal sites.[35] Clearly, the confined space promoted relatively favorable interactions (high localized charge density) between the CO_2 and the framework and subsequently improved the CO_2 adsorption energetics and uptake.[36]

With regard to hydrogen adsorption, Q_{st} of **2** was found to be higher than **1** over the entire adsorption range (*e.g.*, 7.15 *vs.* 6.15 kJ mol^{-1} at low loading); nevertheless, the uptake at 77 K and 1 bar was comparable for **1** and **2** (1.96 *vs.* 1.98 wt%) (ESI, Fig. S12 and S13†). In this case, the observed increase in the H_2
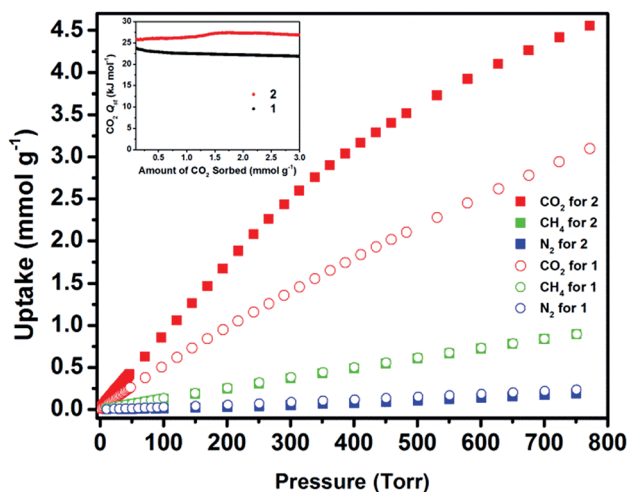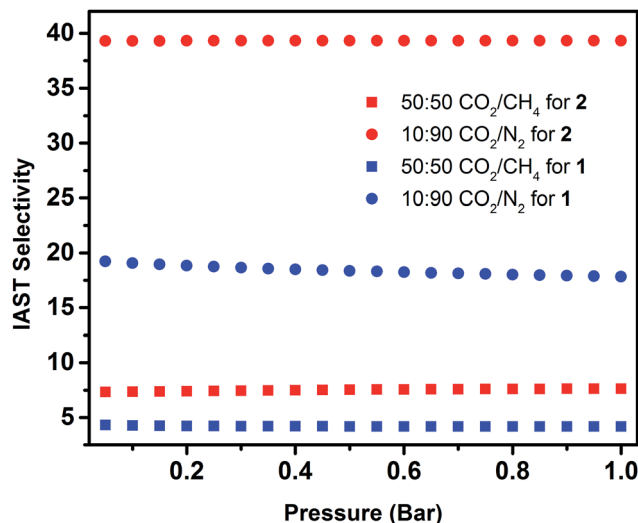

Fig. 5 IAST selectivities for 50 : 50 CO_2/CH_4 (squares) and 10 : 90 CO_2/N_2 (circles) binary mixtures predicted at 298 K for **1** (blue) and **2** (red).

adsorption energetics for **2** can be interpreted as a result of the confined space effect, promoting a higher localized charge density in a more comparatively confined space.[37]

Adsorption studies of CH_4, C_2H_6 and C_3H_8 were conducted in order to evaluate **1** and **2** separation potential of light hydrocarbons.

The C_2H_6 and C_3H_8 adsorption uptake for **1** at 1 bar and 298 K is 5.21 and 5.99 mmol g^{-1}, which are higher than the C_2H_6 and C_3H_8 uptake for **2** (4.31 and 4.77 mmol g^{-1}, respectively) (Fig. 6). This observed enhanced hydrocarbon adsorption uptake for **1** can be attributed to a comparatively larger available total pore volume in **1** relative to **2**. Nevertheless, the predicted adsorption separation factors (using IAST) of **1** and **2** for C_2H_6 and C_3H_8 over CH_4 in 5 : 95 C_2H_6/CH_4 and 5 : 95 C_3H_8/CH_4 binary gas mixtures reveal a slightly higher selectivity for **2**

Fig. 4 Single component gas adsorption isotherms for CO_2, CH_4 and N_2 at 298 K and CO_2 Q_{st} (inset) for **1** and **2**.
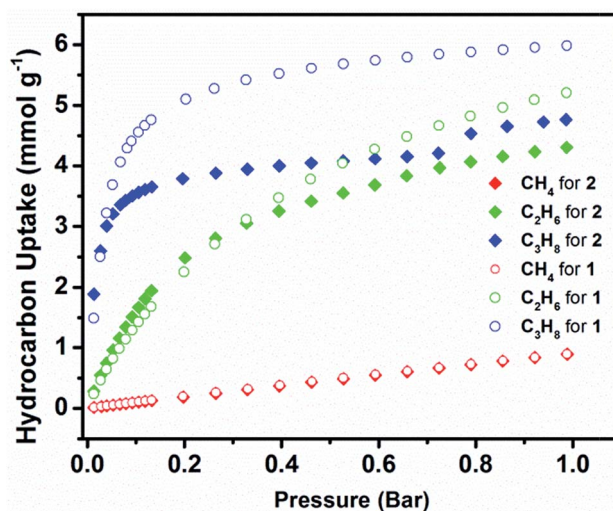
Fig. 6 Single component gas adsorption isotherms for C_3H_8, C_2H_6 and CH_4 at 298 K for **1** and **2**.

This journal is © The Royal Society of Chemistry 2015

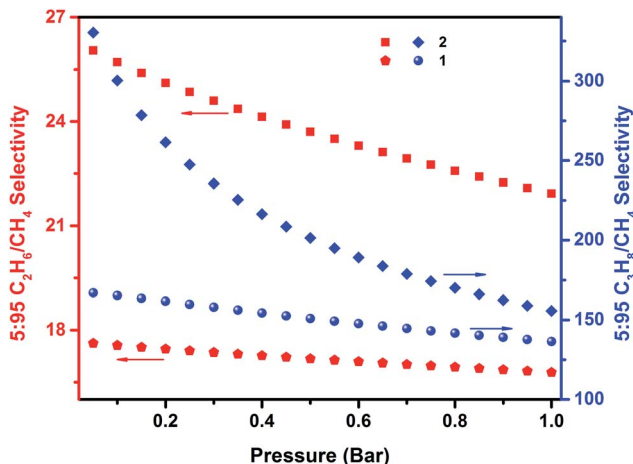*J. Mater. Chem. A*, 2015, **3**, 6276–6281 | **6279**

Fig. 7 IAST selectivities for 5 : 95 C_2H_6/CH_4 (red; left ordinate) and 5 : 95 C_3H_8/CH_4 (blue; right ordinate) binary mixtures predicted at 298 K for **1** and **2**.

(156 and 22, respectively) than **1** (136 and 17, respectively) at 298 K and 1 bar (Fig. 7). These results support, as in the case of the CO_2 separation, the impact of pore size reduction on the affinity enhancement for light hydrocarbons *versus* methane.

3. Conclusions

We have successfully utilized the supermolecular building layer (SBL) approach for the design and construction of isoreticular (3,6)-connected **eea**-MOFs and **rtl**-MOFs. The acylamide-functionalized **eea**-MOF showed a relatively good capacity for CO_2 storage, as well as good selectivity toward CO_2 and C_3H_8 at 298 K. The deliberate pore size reduction resulted in an enhanced local charge density and subsequently an increased CO_2 uptake at both relatively low pressures (0.15 bar) and atmospheric pressures. Light hydrocarbon separation studies suggest that C_2H_6 and C_3H_8 could be selectively removed from natural gas to produce a relatively valuable commodity such as CH_4. This MOF platform, based on the ligand-to-axial (L-A) pillaring approach, offers opportunities to readily functionalize and fine-tune the MOF pores with moieties that can favorably interact with a given probe molecule and subsequently provide access to functional MOF materials with improved attributes for gas separation and storage.

Acknowledgements

Notes and references

1 K. Sumida, D. L. Rogow, J. A. Mason, T. M. McDonald, E. D. Bloch, Z. R. Herm, T.-H. Bae and J. R. Long, *Chem. Rev.*, 2011, **112**, 724–781.
2 O. K. Farha, A. O. Yazaydın, I. Eryazici, C. D. Malliakas, B. G. Hauser, M. G. Kanatzidis, S. T. Nguyen, R. Q. Snurr and J. T. Hupp, *Nat. Chem.*, 2010, **2**, 944–948.
3 P. Nugent, Y. Belmabkhout, S. D. Burd, A. J. Cairns, R. Luebke, K. Forrest, T. Pham, S. Ma, B. Space, L. Wojtas, M. Eddaoudi and M. J. Zaworotko, *Nature*, 2013, **495**, 80–84.
4 E. D. Bloch, W. L. Queen, R. Krishna, J. M. Zadrozny, C. M. Brown and J. R. Long, *Science*, 2012, **335**, 1606–1610.
5 H. Wu, Q. Gong, D. H. Olson and J. Li, *Chem. Rev.*, 2012, **112**, 836–868.
6 Z. Zhang, Z.-Z. Yao, S. Xiang and B. Chen, *Energy Environ. Sci.*, 2014, **7**, 2868–2899.
7 Y. Peng, V. Krungleviciute, I. Eryazici, J. T. Hupp, O. K. Farha and T. Yildirim, *J. Am. Chem. Soc.*, 2013, **135**, 11887–11894.
8 J. Liu, L. Chen, H. Cui, J. Zhang, L. Zhang and C.-Y. Su, *Chem. Soc. Rev.*, 2014, **43**, 6011–6061.
9 S. Qiu, M. Xue and G. Zhu, *Chem. Soc. Rev.*, 2014, **43**, 6116–6140.
10 M. C. So, M. H. Beyzavi, R. Sawhney, O. Shekhah, M. Eddaoudi, S. S. Al-Juaid, J. T. Hupp and O. K. Farha, *Chem. Commun.*, 2015, **51**, 85–88.
11 D. Cunha, M. B. Yahia, S. Hall, S. R. Miller, H. Chevreau, E. Elkaïm, G. Maurin, P. Horcajada and C. Serre, *Chem. Mater.*, 2013, **25**, 2767–2776.
12 J. An, S. J. Geib and N. L. Rosi, *J. Am. Chem. Soc.*, 2009, **131**, 8376–8377.
13 P. Horcajada, R. Gref, T. Baati, P. K. Allan, G. Maurin, P. Couvreur, G. Férey, R. E. Morris and C. Serre, *Chem. Rev.*, 2012, **112**, 1232–1268.
14 M. Eddaoudi, D. B. Moler, H. Li, B. Chen, T. M. Reineke, M. O'Keeffe and O. M. Yaghi, *Acc. Chem. Res.*, 2001, **34**, 319–330.
15 M. O'Keeffe, M. A. Peskov, S. J. Ramsden and O. M. Yaghi, *Acc. Chem. Res.*, 2008, **41**, 1782–1789.
16 O. Shekhah, Y. Belmabkhout, Z. Chen, V. Guillerm, A. Cairns, K. Adil and M. Eddaoudi, *Nat. Commun.*, 2014, **5**, 4228.
17 X. Duan, R. Song, J. Yu, H. Wang, Y. Cui, Y. Yang, B. Chen and G. Qian, *RSC Adv.*, 2014, **4**, 36419–36424.
18 Y. Belmabkhout, H. Mouttaki, J. F. Eubank, V. Guillerm and M. Eddaoudi, *RSC Adv.*, 2014, **4**, 63855–63859.
19 Z. R. Herm, E. D. Bloch and J. R. Long, *Chem. Mater.*, 2014, **26**, 323–338.
20 V. Guillerm, D. Kim, J. F. Eubank, R. Luebke, X. Liu, K. Adil, M. S. Lah and M. Eddaoudi, *Chem. Soc. Rev.*, 2014, **43**, 6141–6172.
21 J. F. Eubank, L. Wojtas, M. R. Hight, T. Bousquet, V. C. Kravtsov and M. Eddaoudi, *J. Am. Chem. Soc.*, 2011, **133**, 17532–17535.
22 S. Xiang, J. Huang, L. Li, J. Zhang, L. Jiang, X. Kuang and C.-Y. Su, *Inorg. Chem.*, 2011, **50**, 1743–1748.
23 X. Liu, M. Oh and M. S. Lah, *Inorg. Chem.*, 2011, **50**, 5044–5053.
24 X. Liu, M. Oh and M. S. Lah, *Cryst. Growth Des.*, 2011, **11**, 5064–5071.
25 J. F. Eubank, H. Mouttaki, A. J. Cairns, Y. Belmabkhout, L. Wojtas, R. Luebke, M. Alkordi and M. Eddaoudi, *J. Am. Chem. Soc.*, 2011, **133**, 14204–14207.
26 H. Li, M. Eddaoudi, T. L. Groy and O. M. Yaghi, *J. Am. Chem. Soc.*, 1998, **120**, 8571–8572.

6280 | *J. Mater. Chem. A*, 2015, **3**, 6276–6281

This journal is © The Royal Society of Chemistry 2015

27 B. Zheng, H. Liu, Z. Wang, X. Yu, P. Yi and J. Bai, *CrystEngComm*, 2013, **15**, 3517–3520.

28 K. Tang, R. Yun, Z. Lu, L. Du, M. Zhang, Q. Wang and H. Liu, *Cryst. Growth Des.*, 2013, **13**, 1382–1385.

29 B. Zheng, J. Bai, J. Duan, L. Wojtas and M. J. Zaworotko, *J. Am. Chem. Soc.*, 2010, **133**, 748–751.

30 Y. Xiong, Y.-Z. Fan, R. Yang, S. Chen, M. Pan, J.-J. Jiang and C.-Y. Su, *Chem. Commun.*, 2014, **50**, 14631–14634.

31 R. Vaidhyanathan, S. S. Iremonger, K. W. Dawson and G. K. H. Shimizu, *Chem. Commun.*, 2009, 5230–5232.

32 N. Planas, A. L. Dzubak, R. Poloni, L. C. Lin, A. McManus, T. M. McDonald, J. B. Neaton, J. R. Long, B. Smit and L. Gagliardi, *J. Am. Chem. Soc.*, 2013, **135**, 7402–7405.

33 A. L. Myers and J. M. Prausnitz, *AIChE J.*, 1965, **11**, 121–127.

34 Y. Belmabkhout and A. Sayari, *Chem. Eng. Sci.*, 2009, **64**, 3729–3735.

35 S. D. Burd, S. Ma, J. A. Perman, B. J. Sikora, R. Q. Snurr, P. K. Thallapally, J. Tian, L. Wojtas and M. J. Zaworotko, *J. Am. Chem. Soc.*, 2012, **134**, 3663–3666.

36 L. Du, Z. Lu, K. Zheng, J. Wang, X. Zheng, Y. Pan, X. You and J. Bai, *J. Am. Chem. Soc.*, 2012, **135**, 562–565.

37 Y. Liu, J. F. Eubank, A. J. Cairns, J. Eckert, V. C. Kravtsov, R. Luebke and M. Eddaoudi, *Angew. Chem., Int. Ed.*, 2007, **46**, 3278–3283.

This journal is © The Royal Society of Chemistry 2015

J. Mater. Chem. A, 2015, **3**, 6276–6281 | **6281**